Supporting Information Appendix for

Targeting Collagen Strands by Photo-Triggered Triple Helix Hybridization

Yang Li, Catherine A. Foss, Daniel D. Summerfield, Jefferson J. Doyle, Collin M. Torok, Harry C. Dietz, Martin G. Pomper, S. Michael Yu*

*To whom correspondence should be addressed. E-mail: yu@jhu.edu

This file includes:

SI Materials and Methods

Synthesis of caged CMPs.

Non-caged peptides were synthesized on a 433A peptide synthesizer (Applied Biosystems) using standard Fmoc and HBTU chemistry (1). The caged peptides (0.1 mmol scale) were prepared using combined automated and manual solid phase synthesis (Fig. S2). Fmoc(N-*o*-nitrobenzyl)Gly-OH was synthesized following the modified method of Tatsu et al (2) (Fig. S2*A*). The peptide sequence preceding ^{NB}Gly was synthesized automatically and Fmoc-^{NB}Gly-OH (4 molar equiv) was coupled manually by standard HBTU chemistry. The next amino acid (Fmoc-Hyp(tBu)-OH or Fmoc-$^{L/D}$Pro-OH) was coupled by PyBroP activation: 9 molar equivalent of the amino acid, 8.8 molar equivalent of PyBroP, 20 molar equivalent of DIPEA were added and allowed to react over 24 hr. The coupling efficiency was over 85% as estimated by HPLC. The remaining sequence was completed by automated synthesis, followed by on-resin labeling with 6 molar equivalent of 5(6)-carboxyfluorescein (Sigma) activated by 6 molar equivalent of PyAOP (Sigma) (3). Resins were treated with trifluoroacetic acid (TFA)/triisopropylsilane(TIS)/water (95:2.5:2.5) for 3 hr and the target peptide was precipitated by adding excess cold ether to the TFA solution. Crude peptide products were purified by reverse phase HPLC on a Vydac C18 column using a linear gradient (5-45% B in 40 min) mixture of water (A, 0.1% TFA) and acetonitrile (B, 0.1% TFA). Purified peptides were analyzed by Bruker AutoFlexIII MALDI-ToF (Bruker Daltonics; Table S1).

Circular dichroism spectroscopy.

CD spectra were collected on JASCO 715 spectrophotometer equipped with a JASCO PTC-348 WI temperature controller and quartz cells (0.1 mm pathlength). CMP solutions (320 μL, 150 μM in 1×PBS) were stored at 4 °C for at least 24 hr before measurement. For photo-decaging, samples were exposed to 365 nm UV light for at least 30 min before the 4 °C incubation. The thermal melting studies were performed by measuring the ellipticity at 225 nm with 60 °C/hr heating rate. Raw CD signal was normalized to mean residue ellipticity based on the peptide's length and concentration (4). Melting temperatures (T_m) were determined by fitting the mean residue ellipticity to a two-state model (5). To measure the refolding kinetics, CMP solution was thermally denatured at 75 °C for 10 min in a cuvette and rapidly quenched to 25 °C in an ice-water bath, after which the CD signal at 225 nm was observed over time at 25 °C. The CD spectra of intact and MMP-1 cleaved type I collagen (Fig. S8) was measured in 90 μg/mL protein solutions in 20 mM acetic acid buffer at 22 °C. The 37 °C thermal stability profile (Fig. 2*E*, inset) was generated by monitoring the ellipticity at 222 nm immediately after transferring the cuvette to a temperature controlled cuvette holder pre-set to 37 °C. The T_m values reported in this study are approximately 10 °C higher than the equilibrium T_m due to high heating rate (60 °C/hr) (6).

Collagen/gelatin binding assays.

Collagen solution (200 μL, 3.71 mg/mL, type I rat tail, BD Science) in 0.02 N acetic acid was added to each well of a 96-well black/clear-bottom plate (Costar) and air-dried. To make gelatin films, the same collagen solution was denatured at 70 °C for 15 min before applying to the well. The dried

films were neutralized and washed with 1×PBS buffer (pH 7.4) and deionized water. PBS solution of carboxyfluorescein-labeled caged CMP (40 μL, 50 μM, unless indicated otherwise) pre-equilibrated at 4 °C was added onto each reconstituted collagen or gelatin film and exposed to 365 nm UV light (10 mW/cm^2, from mercury arc lamp) for 11 min on ice. Wells for the UV-negative control groups were covered with aluminum foil to block UV exposure. After incubation at 4 °C for over 3 hr (unless indicated otherwise), the unbound materials were removed by rinsing with PBS buffer and deionized water. The films were allowed to dry in dark, after which the fluorescence (ex: 489 nm, em: 533 nm) was measured with a SpectraMax Gemini XPS microplate reader (Molecular Devices). Each binding experiment was done in triplicate.

Quantification of CF(GPO)$_9$ bound on type I collagen films.

Following photo-induced binding, CMP-bound collagen films (e.g. the UV+ group of Fig. S6*A*) were digested with 200 μL of collagenase (Sigma, C0130) solutions (1 mg/mL) in TESCA buffer (50 mM TES buffer with 1.36 mM $CaCl_2$, pH 7.4) for 1 hr at 37 °C. The digested solutions were directly used for fluorescence measurement (ex: 489 nm, em: 533 nm). For the standard curve, a series of solutions containing known amounts of CF^{NB}(GPO)$_9$ (0 to 0.35 nmol) were applied to blank collagen films and air-dried, followed by collagenase digestion and fluorescence measurement as described above. The amount of bound CF(GPO)$_9$ was determined by comparing the fluorescence intensity of the digested collagen/CMP solutions with the standard curve, and the binding density was determined by dividing the amount bound by the area of the well. The experiment was performed in triplicate.

CMP binding assay on thermally-denatured type I and II collagens.

A solid-state protein coating instead of a reconstituted gelatin film (as described above) was chosen as the binding substrate to avoid the collagen type dependent film instability. Wells of nunc black 96-well maxisorp plate (Thermo Scientific) were charged with 50 μL of 1×PBS buffer containing 100 μg/mL type I or type II (bovine, BD Science) collagen which was denatured by 10 min of incubation at 75 °C. After 1 hr, the coating solutions were removed and wells were washed with 1×PBS buffer containing 1 mg/mL BSA (PBSB), and blocked with 50 mg/mL BSA in PBS for 1 hr, followed by additional wash with PBSB. CF^{NB}(GPO)$_9$ or CF^{S}G$_9$P$_9$O$_9$ solution (20 μM, 50 μL in PBS) was added to each well, exposed to UV light for 10 min, and incubated at room temperature for 2.5 hr. Wells were washed three times with 100 μL of PBSB followed by fluorescence (ex: 489 nm, em: 533 nm) reading with a SpectraMax M-2 microplate reader (Molecular Devices). Each binding experiment was done in triplicate. The background fluorescence of empty wells was subtracted from the raw fluorescence data.

Photo-patterning of collagen and gelatin films.

On the lid of a 48-well cell culture plate (Costar), 150 μL of type I collagen solution (3.71 mg/mL) was evenly applied and enclosed with a condensation ring (diameter: 11 mm). The solution was allowed to dry and washed three times with PBS to form a collagen film. Gelatin films were made in the same way using denatured type I collagen which was pre-incubated at 70 °C for 15 min.

$CF^{NB}(GPO)_9$ solution (100 μL, 200 μM in 1×PBS) was applied to each film and incubated at room temperature for 20 min. Excess CMP solution was removed, leaving collagen/gelatin films swollen in $CF^{NB}(GPO)_9$. A transparency mask was carefully mounted on top of the condensation ring and the films were exposed to UV light (365 nm) through the transparency mask for 12 min at 4 °C, followed by 1 hr incubation to allow peptide binding. The films were washed with deionized water and imaged by Gel Doc EQ system (BioRad).

MMP-1 digestion of type I collagen and CMP binding assays.

ProMMP-1 (1 μg, EMD Millipore) was activated by p-aminophenylmercuric acetate (1.1 mM) in 132.5 μL of TNC buffer (50 mM Tris-HCl, 0.15 M NaCl, 5 mM $CaCl_2$, 0.02% NaN_3, pH 7.5) at 37 °C for 3 hr. Type I collagen (62.6 μg) was subsequently added to the MMP-1 solution and incubated at room temperature for at least 3 days. Digested products were analyzed by SDS-PAGE and circular dichroism spectroscopy (Fig. S8). Wells of nunc black 96-well maxisorp plate were charged with 50 μL of TNC buffer containing 0.5 M glycerol, and 100 μg/mL collagen or MMP-1 cleaved collagen, and incubated at room temperature. The collagen solutions used were either kept at room temperature (22 °C) or incubated at 37 °C for 1 min just prior to coating. After 2.5 hr, the coating solutions were removed and wells were washed with PBSB (1 mg/mL BSA in 1×PBS) and blocked with 50 mg/mL BSA in PBS for 1 hr, followed by additional wash with PBSB. $CF^{NB}(GPO)_9$ solution (20 μM, 50 μL in PBS) was added to each well, exposed to UV light for 10 min, and incubated at room temperature for 2.5 hr. Wells were washed extensively with PBSB followed by fluorescence (ex: 489 nm, em: 533 nm) reading with a SpectraMax M-2 microplate reader (Molecular Devices). Each binding experiment was done in triplicate. The background fluorescence of empty wells was subtracted from the raw fluorescence data. For estimating the amount of adsorbed protein, un-blocked collagen-coated wells were treated with 100 μM 5-(4,6-dichlorotriazinyl)aminofluorescein (DTAF, 50 μL, in 0.1 M sodium borate buffer) at room temperature for 3 hr, and the fluorescence (ex: 489 nm, em: 533 nm) of the well was measured after washing with 1×PBS. For each collagen substrates, fluorescence from the CMP binding was normalized by the fluorescence from the DTAF staining to calculate the relative CMP binding level per protein.

Staining of SDS-PAGE gels using photo-decaged $CF(GPO)_9$.

MMP-1 digested type I collagen (3.5 μg) was separated by SDS-PAGE (4-12% polyacrylamide gel) under non-reducing condition, along with unstained protein ladder (Life technologies, LC5801). After washing, the gel was soaked in 6 μM $CF^{NB}(GPO)_9$ (or $CF^{S}G_9P_9O_9$) in 1×PBS solution, followed by exposure to 365 nm UV light for 15 min, and 2.5 hr of staining. The gel was washed with deionized water and scanned using Typhoon 9410 Imager (GE Healthcare) with 488 nm fluorescence channel. Afterwards, the protein gel was stained by coomassie brilliant blue and imaged by Gel Doc EQ system (BioRad).

Labeling CMPs with near infrared fluorescent dyes.

Caged Cys-Ahx-$^{NB}(GPO)_9$ [C-Ahx-$(GPO)_4{}^{NB}GPO(GPO)_4$] and scrambled peptide Cys-Ahx-

$^{S}G_9P_9O_9$ (C-Ahx-PGOGPGPOPOGOGOPPGOOPGGOOPPG) were synthesized using the SPPS protocol as described above. After the acetylation of the N-terminal amines, the peptides were cleaved from the resin with TFA/TIS/1,2-ethanedithiol/water (94:1:2.5:2.5). After HPLC purification (MADLI in Table S1), both peptides (~1.2 mg for each labeling reaction) were labeled with 0.25 mg of either IRDye 680RD maleimide or IRDye 800CW maleimide (LI-COR Biosciences) in 300 μL of 3×PBS buffer at 4 °C overnight and further purified by HPLC on a Vydac C18 column using a linear gradient (13-30% B in 34 min) mixture of water (A, 0.1% TFA) and acetonitrile (B, 0.1% TFA).

***In vivo* tumor targeting.**

All animal studies were undertaken in compliance with the regulations of the Johns Hopkins Animal Care and Use Committee. Both prostate-specific membrane antigen (PSMA) expressing (PC3-PIP) and non-PSMA expressing (PC3-flu) PC-3 prostate cancer cell lines were grown in RPMI 1640 medium (Invitrogen) containing 10% fetal bovine serum (FBS) and 1% Pen-Strep (Biofluids). Eight- to twelve-week-old male, non-obese diabetic (NOD)/severe-combined immunodeficient (SCID) mice (JHU Cancer Center) were implanted subcutaneously with PC3-PIP and PC3-flu cells (1×10^6 in 50 μL of HBS) behind the right and left forearms, respectively. Mice were used for *in vivo* tests when the xenografts reached 5-7 mm in diameter. Hair remover was applied to the entire ventral tumor region in both mice to enhance imaging. Saline solution (100 μL) containing 3.7 nmol of IR-Ahx-$^{NB}(GPO)_9$ and 1 nmol of cysteine (for quenching photo cleaved aldehyde byproduct) sitting at approximately 40 °C was exposed to UV light (365 nm, >25 mW/cm^2) for 5 min and immediately injected to the mouse intravenously *via* the lateral tail vein. Control peptide IR-Ahx-$^{S}G_9P_9O_9$ was injected into the second mouse following the identical procedure. Images, shown in rainbow format, were acquired at designated times using a Pearl Impulse Imager (LI-COR Biosciences) with fixed excitation (785 nm) and fluorescence emission wavelengths (800 nm). The same procedures were performed on another pair of NOD-SCID mice bearing two subcutaneous PC3-PIP tumors. One dose of MMPSense 680^{TM} (2 nmol in 150 μL 1×PBS, PerkinElmer) was administered to each mouse *via* tail vein 80 hr post CMP injection. After 22 hr (corresponding to 102 hr PI of CMP), the mice were imaged at both 710 nm (MMPSense) and 800 nm (CMP). The mice were sacrificed by cervical dislocation and their internal organs exposed to allow imaging of deep tissues.

Murine Panc02 and human Panc198 cells were acquired from the ATCC (Rockville, MD) and cultured in RPMI1640 supplemented with 10% FBS, 10 μg/mL of streptomycin and 10 I.U./mL of penicillin at 37 °C in 5% CO_2 and humidified air until 80-95% confluence. The cells were then trypsinized and formulated at either 2×10^6 cells/100 μL (Panc198) or 1×10^6 cells/100 μL (Panc02) followed by subcutaneous inoculation into 12-week-old female athymic nu/nu mice (NCI). Panc198 and Panc02 cells were inoculated subcutaneously behind the left and right shoulder, respectively. When the Panc02 xenograft reached 4-6 mm in diameter (~2 weeks after inoculation), each mouse was intravenously administered with solution containing 4 nmol of photo-activated IR-Ahx-$(GPO)_9$ or IR-Ahx-$^{S}G_9P_9O_9$ and 1 nmol of cysteine, followed by MMPsense injection and NIRF imaging as described. Both mice's Panc02 and Panc198 tumors as well as the legs which showed CMP uptake

were harvested and imaged (Fig. S11).

***In vivo* skeleton targeting.**

PBS solution (100 μL) containing 4 nmol of IR′-Ahx-$^{NB}(GPO)_9$ or IR′-Ahx-$^{S}G_9P_9O_9$, and 1 nmol of cysteine equilibrated at 37 °C was exposed to UV light (365 nm, >25 mW/cm^2) for 5 min and immediately injected to a male BALB/c mouse (about 9 weeks old) *via* tail vein. One dose of IRDye800CW BoneTag^{TM} (10 nmol, LI-COR Biosceinces) was administered to each mouse *via* tail vein ~72 hr post CMP injection. After 24 hr (corresponding to 96 hr PI of CMP), the mice were sacrificed by cervical dislocation and their skins were removed to allow imaging of deep tissues. Major organs and the skeleton were harvested and imaged by a Pearl Impulse Imager at both 710 nm (CMP) and 800 nm (BoneTag).

Ex vivo hind limb and right hemisphere of ribs were manually stripped of most skeletal muscle and scanned laterally using a LI-COR Odyssey imager set to 23 micron resolution in both the 710 nm (CMP) and 800 nm (BoneTag) channels. The resulting images were processed using the Odyssey software to generate single channel and merged images (Fig. 4*C*, Fig. S13*B*, ribs and knee).

The same CMP injection and imaging procedure was performed in 12-month old Marfan mice, developed as reported in ref. (7), as well as age- and gender-matched wild type littermates (Fig. 4*E*).

***In vivo* control peptide studies.**

IR′-Ahx-$^{NB}(GPO)_9$ (4 nmol) and 1 nmol of cysteine in 100 μL of PBS was exposed to UV light for 5 min and immediately injected to CD1 nude mice *via* tail vein (Fig. 4*B*, panel i). Another mouse was injected with the same solution without the UV exposure (Fig. 4*B*, panel ii). For the third mouse, IR′-Ahx-$^{NB}(GPO)_9$ was fully de-caged by UV and allowed to fold into triple helix at 4 °C for over 48 hr before injection (Fig. 4*B*, panel iii). The whole body scan was taken at 96 hr PI using a Pearl Impulse Imager after skin removal as previously described.

***Ex vivo* immunofluorescence histology of the tumors and the knee cartilage.**

PC-3 tumors were harvested and cryosectioned to 20 μm thickness on charged glass slides without any chemical fixation. The unfixed slides were probed with anti-CD31-PE antibody conjugate (Abcam, ab25644, 1:67) and anti-Col 2 $^3/_4C_{short}$ antibody (IBEX, 50-1035, 1:100) in 10% FBS (Sigma) in PBS for 1 hr at room temperature. The anti-collagen antibody was detected with a secondary anti-rabbit-AlexaFluor488 immunoconjugate (Invitrogen, A11070, 1:250). The slides were washed and covered with glass cover slips.

Legs of mice from *in vivo* PanC tumor targeting experiment (see above and Fig. S11) were harvested and frozen on dry ice following 96 hr NIRF imaging. The legs were stored at -80 °C until brief thawing and manual recovery of knee cartilage for subsequent cryosectioning. Cartilage specimens were sectioned to 15 μm thickness using an HM 550 cryotome and transferred onto charged glass microscope slides (VWR Superfrost). The sections were probed with rabbit anti-Col 2 $^3/_4C_{short}$ antibody (1:40) in 10% FBS in PBS for 1 hr at room temperature, followed by secondary anti-rabbit-AlexaFluor488 immunoconjugate (1:250) in PBS and 1 ng/mL of Hoecst 33342 dye

(Fisher Scientific) in PBS, before washing and mounting. All images were recorded and processed using a Nikon 80i epifluorescence microscope with Nikon Imaging Software Elements. CMP images (800 nm) were acquired over a standardized 8 sec exposure time.

SI Text

Photo-triggered CMP binding to the intact type I collagen.

To study the photo-triggered binding affinity of the caged CMP to intact type I collagen films, $CF^{NB}(GPO)_9$ was applied to a 96-well assay microplate coated with reconstituted type I collagen films, and binding levels were determined with and without UV exposure by measuring the fluorescence intensity of the collagen films after washing. The entire binding assay was conducted at 4 °C to prevent thermal denaturation of the collagen films. As shown in Fig. S6*A*, collagen binding was observed only after exposing the sample to UV light. We also tested the photo-triggered binding of a non-caged, triple helical $CF(GPO)_9$. In this control experiment, CMP binding was lower by a factor of 11 compared to the UV-triggered binding of the $CF^{NB}(GPO)_9$ (Fig. S6*A*, last bar). The results confirmed that CMP binding to intact collagen films is real and the triple helical folding capacity is crucial for the binding.

Similar to the gelatin binding results, CMP with left handed twist $CF^{NB}(G^DP^DP)_9$ exhibited lower levels of UV triggered collagen binding at 4 °C, only about one fourth of that of $CF^{NB}(GPP)_9$ (Fig. S6*B*, last two bars), confirming that the binding is not simply due to non-specific physical trapping, but it is primarily driven by stereo-selective CMP-collagen hybridization, most likely in the form of a triple helix.

Finally, we compared heat- and UV-induced CMP binding to collagen films directly. As seen in Fig. S7, thermally melted non-caged $CF(GPO)_9$ showed significantly elevated binding levels compared to photo-triggered caged $CF^{NB}(GPO)_9$, suggesting that in our prior work (1, 8, 9) heat facilitated the hybridization process by partially denaturing the collagen *in situ*.

SI Figures

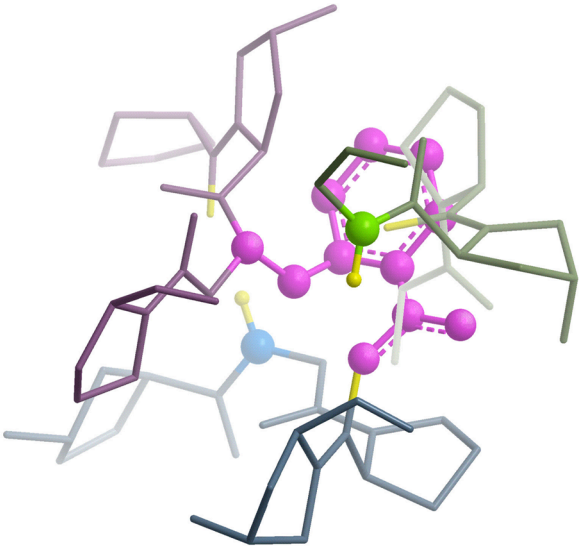

Fig. S1. Computer-generated image (viewed in the direction of the helical axis) of a hypothetical CMP [$(GlyProHyp)_x$] triple helix. Single NB-cage substitution on Gly nitrogen on one CMP strand is shown in purple ball-and-stick model, highlighting the steric clashes with the neighboring chains.

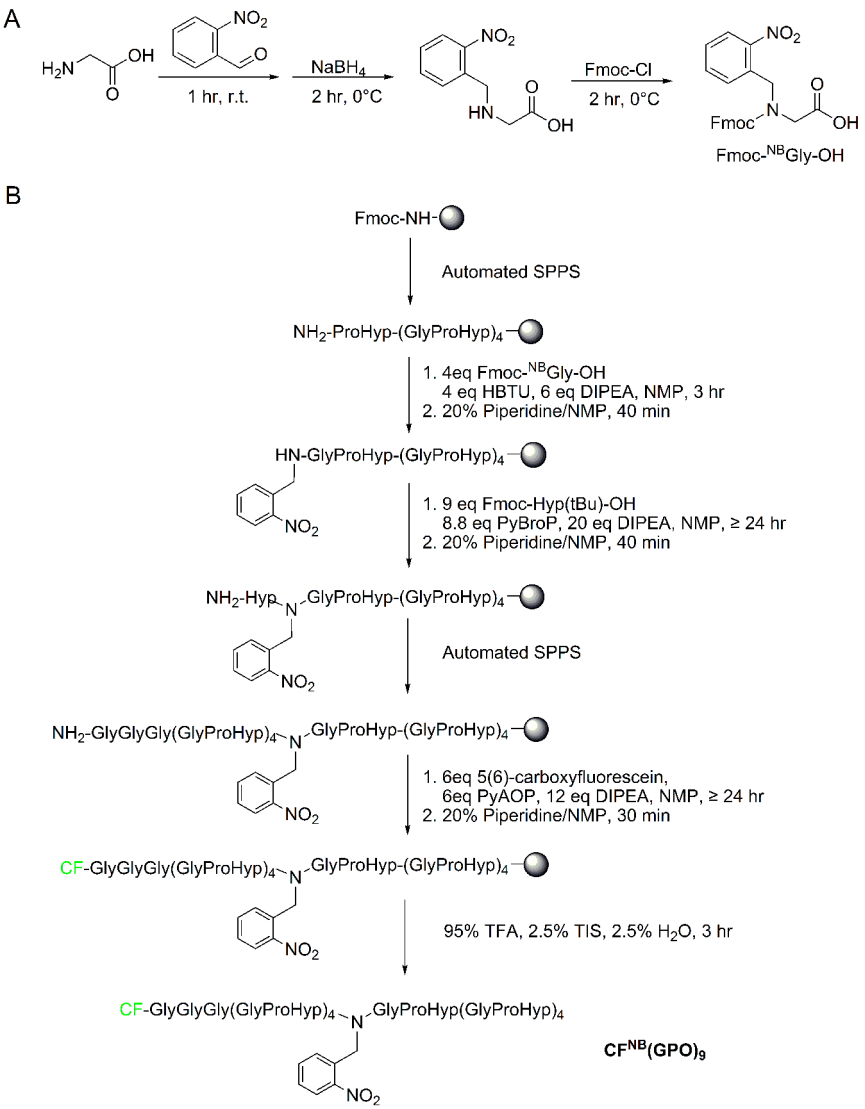

Fig. S2. Synthesis of $CF^{NB}(GPO)_9$. (*A*) Fmoc(N-*o*-nitrobenzyl)Gly-OH was synthesized according to Tatsu et al. (2) with slight modifications: when conjugating Fmoc group onto *N*-2′-nitrobenzyl-glycine, a solution of 1.05 equivalent (1.94 g, 7.5 mmol) of fluorenylmethyloxy chloroformate (Fmoc-Cl) in 10 mL of acetone was added in a drop-wise fashion over 30 min to N-2′-nitrobenzyl-glycine (1 eq, 1.50 g, 7.14 mmol) dissolved in a mixture of 67 mL 3% $NaHCO_3$ and 53.6 mL of acetone vigorously stirring in an ice bath. The reaction mixture was stirred for another 1.5 hr followed by work-up as reported in ref. 6, producing 2.24 g (yield: 73%) of final product. (*B*) Combined automated and manual solid phase synthesis of $CF^{NB}(GPO)_9$. Fluorescent tag, 5(6)-carboxyfluorescein was conjugated to the N-terminus of the peptide on resin using PyAOP and DIPEA followed by piperidine treatment (3, 10, 11).

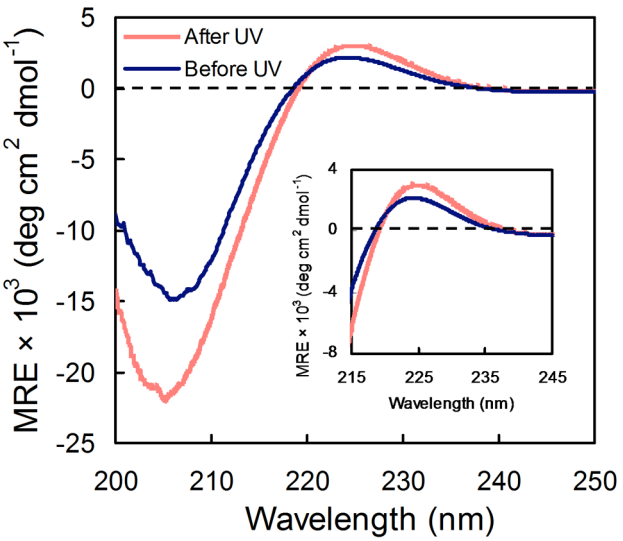

Fig. S3. CD spectra of $CF^{NB}(GPO)_9$ solutions (150 μM in 1×PBS) at 4 °C before and after UV exposure. Both samples were incubated at 4 °C for at least 24 hr before CD measurement to ensure folding. The CD spectrum of $CF^{NB}(GPO)_9$ before UV exposure at 4 °C showed a reduced positive peak near 225 nm (highlighted in inset) and a negative peak at 205 nm, suggesting a polyproline II helix conformation.

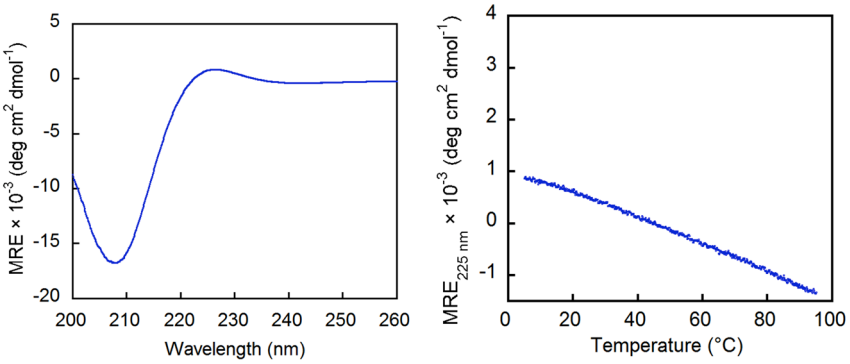

Fig. S4. CD spectrum (left) and melting curve (right) of $CF^{S}G_9P_9O_9$ solutions (150 μM in 1×PBS). The low peak ellipticity value at 225 nm and the linear ellipticity decrease during thermal melting indicate lack of triple helical structure. Samples were incubated at 4 °C for at least 24 hr before CD measurement to ensure folding.

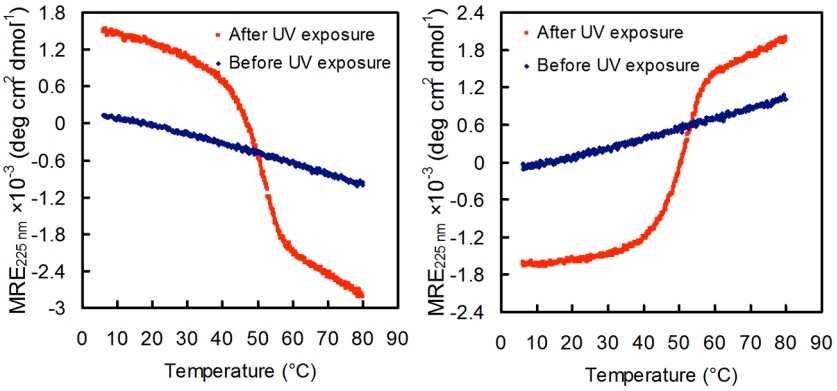

Fig. S5. CD melting curves of $CF^{NB}(GPP)_9$ (left) and $CF^{NB}(G^DP^DP)_9$ (right) before and after UV exposure. Both peptides transformed from single stranded state to folded state after UV exposure, forming triple helices of identical T_m at 51 °C, but of opposite helical twist as evidenced by the mean residue ellipticity values of opposite signs. All samples were incubated at 4 °C for at least 24 hr before CD measurement to ensure folding.

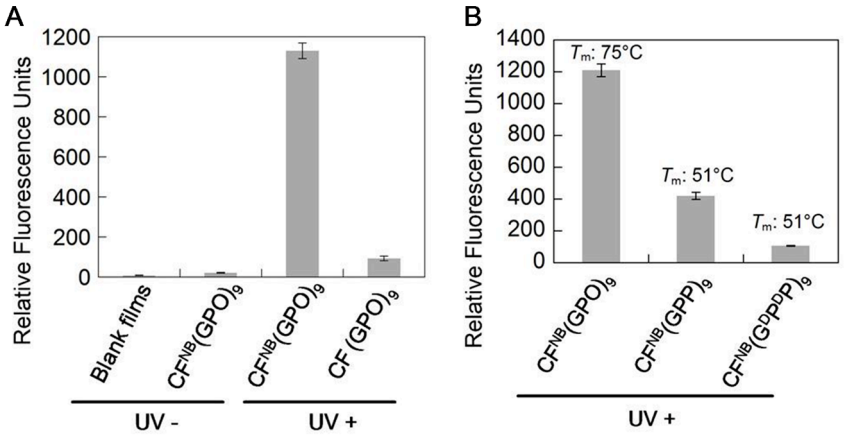

Fig. S6. Photo-triggered CMP binding to intact type I collagens. (*A*) Fluorescence levels of type I collagen films (fibrillar collagen) treated with $CF^{NB}(GPO)_9$ (40 μL/well, 100 μM in 1×PBS, with and without UV exposure) and triple helical $CF(GPO)_9$ (40 μL/well, 100 μM in 1×PBS, pre-equilibrated at 4 °C, with UV exposure). (*B*) Fluorescence levels of type I collagen films (fibrillar collagen) treated with CMP derivatives after UV-induced binding. $CF^{NB}(GPO)_9$, $CF^{NB}(GPP)_9$ and $CF^{NB}(G^DP^DP)_9$ (40 μL/well, 100 μM in 1×PBS) were decaged by UV irradiation directly on collagen films. The CMPs were incubated on collagen films overnight to ensure folding due to the low folding rate of the Hyp-free CMPs. The low collagen binding of $CF(G^DP^DP)_9$ compared to $CF(GPP)_9$ despite nearly identical CD melting behavior suggests that CMP-collagen binding involves multiplex hybridization (most likely in a triple helix form) that is sensitive to the stereochemistry of individual strands. All CMP binding assays were performed at 4 °C in triplicate (±s.d.).

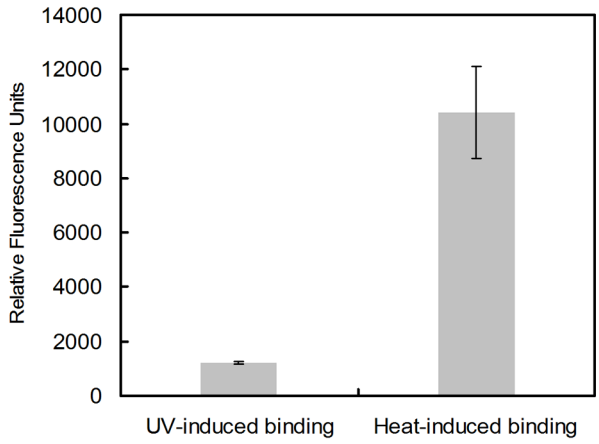

Fig. S7. Fluorescence levels of CF(GPO)$_9$ immobilized on collagen films (fibrillar collagen) by UV- or heat-induced binding. To trigger binding, non-caged CF(GPO)$_9$ (40 μL/well, 100 μM in 1×PBS) was first melted at 75 °C for 10 min and applied to collagen films (heat-induced), while the same amount of CF^{NB}(GPO)$_9$ was exposed to UV light for 22 min on top of collagen films at room temperature (UV-induced). Both collagen films were then incubated for 3 hr at 4 °C to ensure CMP binding. Adding heated non-caged CF(GPO)$_9$ directly to collagen films resulted in significantly higher binding level than the photo-triggered binding due to the heat-induced denaturation of the collagen substrates. The binding assays were performed in triplicate (±s.d.).

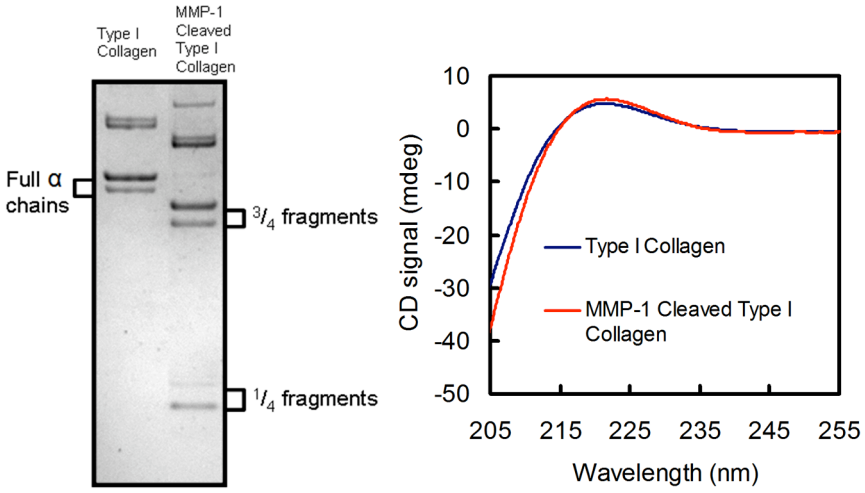

Fig. S8. Characterization of MMP-1 cleaved type I collagen. Left: SDS-PAGE and coomassie brilliant blue staining of MMP-1 cleaved collagen, showing the 3/4 and 1/4 fragments and no residual full length α chains, indicating almost complete digestion. Right: CD spectra of collagen and MMP-1 cleaved collagen (90 μg/mL) in 20 mM acetic acid buffer at 22 °C displaying their similar triple helical contents.

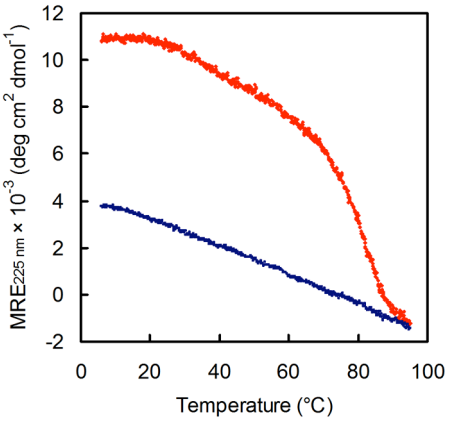

Fig. S9. CD thermal melting curves of photo-decaged IR-Ahx-$^{NB}(GPO)_9$ (red) and IR-Ahx-$^{S}G_9P_9O_9$ (blue, scrambled sequence). IR-Ahx-$^{S}G_9P_9O_9$ exhibited no triple helix forming capacity, while IR-Ahx-$^{NB}(GPO)_9$ demonstrated the expected folding propensity, forming CMP homotrimer with T_m above 75 °C after decaging. All samples were incubated at 4 °C for at least 24 hr before CD measurement to ensure folding.

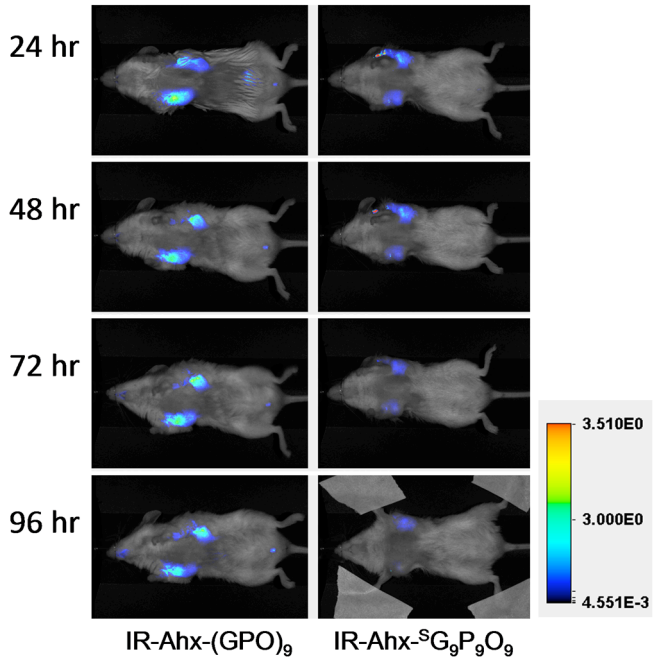

Fig. S10. *In vivo* fluorescence images of NOD/SCID mice bearing PC3-PIP (forward right flank) and PC3-flu (forward left flank) tumors. A pair of NOD/SCID mice were dosed with either 3.7 nmol of photo-decaged IR-Ahx-$^{NB}(GPO)_9$ or same amount of IR-Ahx-$^{S}G_9P_9O_9$. Nair hair remover product was used on the entire ventral tumor region in both mice to remove fur and enhance optical imaging. Ventral views of both mice were obtained at 24 hr, 48 hr, 72 hr, and 96 hr post injection (PI). Photo-activated IR-Ahx-$^{NB}(GPO)_9$ was specifically retained by both tumors through 96 hr PI while the scrambled CMP, IR-Ahx-$^{S}G_9P_9O_9$ was cleared out.

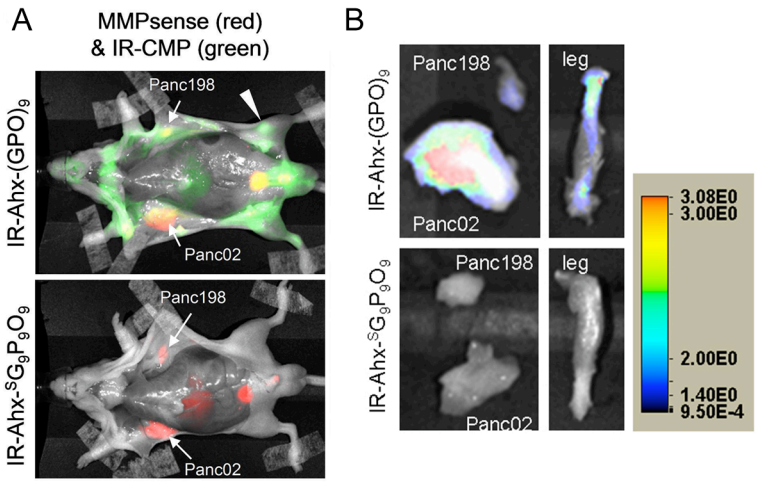

Fig. S11. NIRF images of pancreatic cancer tumors targeted by CMPs. A pair of athymic nu/nu mice bearing Panc02 (forward right flank) and Panc198 (forward left flank) tumors (arrows) were administered with approximately 4 nmol of photo-decaged IR-Ahx-$^{NB}(GPO)_9$ or same amount of IR-Ahx-$^{S}G_9P_9O_9$ *via* tail vein injection. (*A*) Ventral views of the mice after midline surgical laparotomy at 96 hr post CMP injection and 24 hr post MMPSense 680 injection, showing the co-localization (in yellow) of MMP activity (red) and CMP binding (green) in the tumors and surrounding tissues as well as the CMP uptake in the knee joint (arrow head). The mouse injected with IR-Ahx-$^{S}G_9P_9O_9$ showed no peptide accumulation and only MMPSense signal is seen. (*B*) Images of the harvested tumors and legs (containing tibias with femur heads) from both mice, showing uptake of only IR-Ahx-$(GPO)_9$. Fluorescence intensity is shown in rainbow scale with images scaled to the same exposure time.

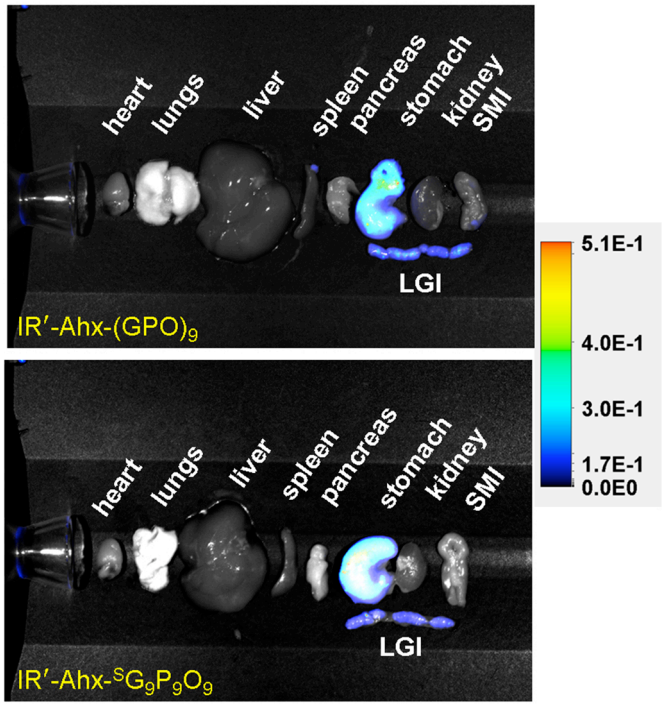

Fig. S12. Organ distribution of CMPs in normal BLAB/c mice. NIRF images (96 hr post injection) of individually harvested organs from two normal BLAB/c mice each administered with 4 nmol of either photo-decaged IR′-Ahx-$^{NB}(GPO)_9$ or same amount of IR′-Ahx-$^{S}G_9P_9O_9$ *via* tail vein injection. No apparent uptake in major organs was observed. The intensity from the stomachs and the intestines (LGI) is due to auto-fluorescence of the chlorophyll in food. Fluorescence intensity is shown in rainbow scale with images scaled to the same exposure time. SMI: small intestine; LGI: large intestine.

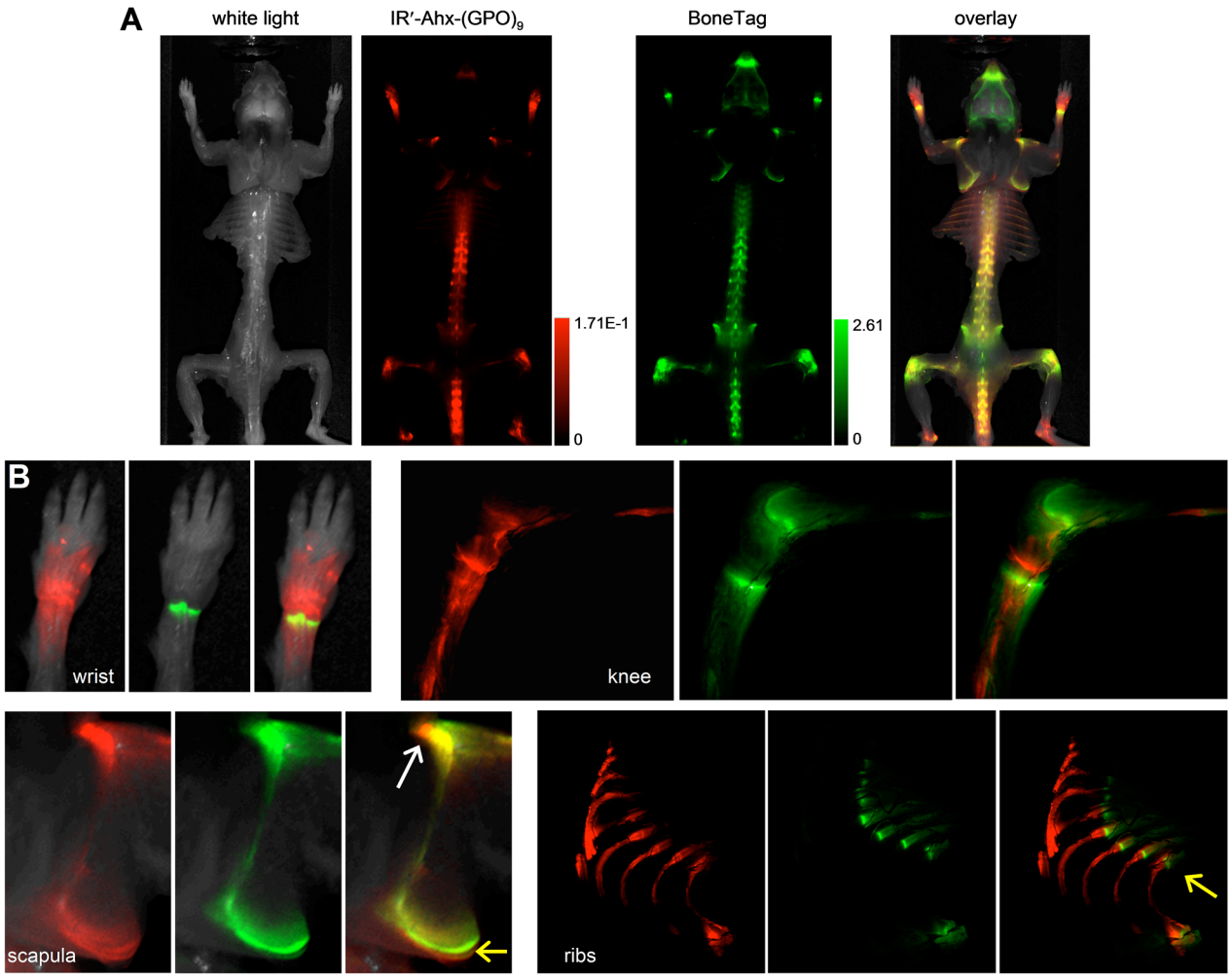

Fig. S13. (*A*) White light and NIRF dorsal images of the same BLAB/c mouse shown in Fig. 4*A*,*C* and Fig. S12, after removing all non-skeletal tissues, demonstrating the similar overall distribution of IR′-Ahx-$(GPO)_9$ (in red), and BoneTag (in green), especially in vertebral spine, knees, wrists, scapulae and maxilla (overlay in yellow). (*B*) High resolution images of separate fluorescence channels indicated that precise locations of these signals are slightly different for the two probes. In the wrist, BoneTag (green) highlights the epiphyseal line of radius and ulna, and CMP (red) shows radius and ulna (lower) and carpal and metacarpal bones. The knee is well defined by intense BoneTag uptake along mineralized bone and colocalizes with CMP at the endochondral junctions while CMP specific uptake can be seen in the articular cartilage and meniscus as well as focal regions within the tibia and the femur head. Details of the scapula views show CMP uptake in articular cartilage (white arrow) and lateral border cartilage (yellow arrow). The costochondral junction (arrow) within the ribs is clearly seen where mineralized bone ends (BoneTag) and cartilaginous ribs begin (CMP). The ribs and knee images were scanned using LI-COR Odyssey imager.

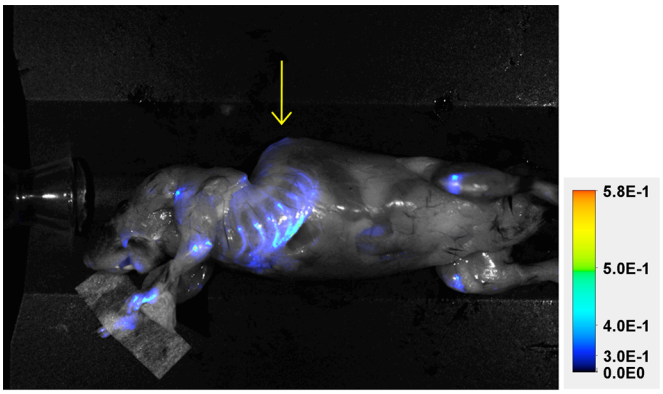

Fig. S14. Lateral view of a mouse model with Marfan's syndrome administrated with 4 nmol of photo-decaged IR′-Ahx-$(GPO)_9$. The mouse was skinned and imaged 96 hr post injection. The white light image showed an apparent kyphosis (yellow arrow), while NIRF signal indicated strong uptake of IR′-Ahx-$(GPO)_9$ in the ribs (intensity shown in rainbow scale).

SI Table

Table S1. Sequence and MALDI-ToF MS of collagen mimetic peptides (CMPs). CF, 5(6)-carboxyfluorescein; O, hydroxyproline; NB, nitrobenzyl; Ac, acetyl; C, cysteine; Ahx, aminohexanoic acid.

CMP	Sequence			*m/z* calculated	*m/z* found
$CF^{NB}(GPO)_9$	CF-GGG-$(GPO)_4{}^{NB}GPO(GPO)_4$	before UV	$[M+Na^+]$	3110.2	3109.4
		after UV	$[M+Na^+]$	2975.1	2974.1
$CF^{NB}(GPP)_9$	CF-GGG-$(GPP)_4{}^{NB}GPP(GPP)_4$	before UV	$[M+Na^+]$	2966.2	2966.6
		after UV	$[M+Na^+]$	2831.1	2831.3
$CF^{NB}(G^DP^DP)_9$	CF-GGG-$(G^DP^DP)_4{}^{NB}G^DP^DP(G^DP^DP)_4$	before UV	$[M+Na^+]$	2966.2	2966.3
		after UV	$[M+Na^+]$	2831.1	2830.9
$CF(GPO)_9$	CF-GGG-$(GPO)_9$		$[M+Na^+]$	2975.1	2975.4
$CF(GPP)_9$	CF-GGG-$(GPP)_9$		$[M+Na^+]$	2831.1	2831.0
$CF(G^DP^DP)_9$	CF-GGG-$(G^DP^DP)_9$		$[M+Na^+]$	2831.1	2831.1
$CF\,{}^{S}G_9P_9O_9$	CF-GGG-PGOGPGPOPOGOGOPPGOOPGGOOPPG		$[M+Na^+]$	2975.1	2973.6
Cys-Ahx-$^{NB}(GPO)_9$	Ac-C-Ahx-$(GPO)_4{}^{NB}GPO(GPO)_4$		$[M+Na^+]$	2839.1	2837.8
Cys-Ahx-$^{S}G_9P_9O_9$	Ac-C-Ahx-PGOGPGPOPOGOGOPPGOOPGGOOPPG		$[M+Na^+]$	2704.0	2703.6

SI References

1. Wang AY, et al. (2008) Spatio-temporal modification of collagen scaffolds mediated by triple helical propensity. *Biomacromolecules* 9:1755-1763.
2. Tatsu Y, Nishigaki T, Darszon A, Yumoto N (2002) A caged sperm-activating peptide that has a photocleavable protecting group on the backbone amide. *FEBS Lett* 525:20-24.
3. Stahl PJ, Cruz JC, Li Y, Yu SM, Hristova K (2012) On-the-resin N-terminal modification of long synthetic peptides. *Anal Biochem* 424:137-139.
4. Li Y, Mo X, Kim D, Yu SM (2011) Template-tethered collagen mimetic peptides for studying heterotrimeric triple-helical interactions. *Biopolymers* 95:94-104.
5. Horng J-C, et al. (2006) Macrocyclic scaffold for the collagen triple helix. *Org Lett* 8:4735-4738.
6. Berisio R, Granata V, Vitagliano L, Zagari A (2004) Characterization of collagen-like heterotrimers: Implications for triple-helix stability. *Biopolymers* 73:682-688.
7. Judge DP, et al. (2004) Evidence for a critical contribution of haploinsufficiency in the complex pathogenesis of Marfan syndrome. *J Clin Invest* 114:172-181.
8. Wang AY, Mo X, Chen CS, Yu SM (2005) Facile modification of collagen directed by collagen mimetic peptides. *J Am Chem Soc* 127:4130-4131.
9. Wang AY, et al. (2008) Immobilization of growth factors on collagen scaffolds mediated by polyanionic collagen mimetic peptides and its effect on endothelial cell morphogenesis. *Biomacromolecules* 9:2929-2936.
10. Fernádez-Carneado J, Giralt E (2004) An efficient method for the solid-phase synthesis of fluorescently labeled peptides. *Tetrahedron Lett* 45:6079-6081.
11. Fischer R, Mader O, Jung G, Brock R (2003) Extending the applicability of carboxyfluorescein in solid-phase synthesis. *Bioconjug Chem* 14:653-660.